PHYSICAL REVIEW B VOLUME 17, NUMBER 2 15 JANUARY 1978

Self-consistent LCAO calculation of the electronic properties of graphite. II. Point vacancy in the two-dimensional crystal

Alex Zunger* and R. Englman
Department of Theoretical Physics and Applied Mathematics, Soreq Nuclear Research Centre, Yavne, Israel

(Received 11 August 1975)

The electronic properties of a point vacancy in the two-dimensional graphite crystal are investigated within the small-periodic-cluster approach using a self-consistent all-valence-electron LCAO (linear combination of atomic orbitals) scheme previously employed for the calculations of the band structure and optical spectra of the regular lattice (part I). Eight crystal bands, 54-96 $\vec{K}$ points in the Brillouin zone, selected according to the "mean value theorem" and 2^2-5^2 primitive unit cells around the defect site are allowed to interact. A doubly degenerate singly occupied σ defect level is shown to appear in the σ-σ^* band gap, 3.5 eV above the σ band edge, with a wave function that is about 80% localized on the three nearest-neighbor atoms. The density of electronic states, charge distribution and Poisson electrostatic potential of the defect structure are computed and used to discuss the characteristic feature of the defect in connection with Coulson's "defect molecule" model and with current models of electron trapping mechanisms used to interpret the experimental data on Hall coefficient, resistivity and diamagnetic susceptibility of damaged graphite. Both symmetric and Jahn-Teller lattice distortions are introduced around the defect site, the results being used to interpret the experimentally observed decrease in lattice constant, the observed optical absorption and the vibronic parameters of the Jahn-Teller effect. Symmetric lattice relaxations are shown to have a moderate effect on the lattice energy and on the position of the defect level, these changes being mainly due to the response of the π subsystem to accumulation of excess π charge on the surrounding bonds, while Jahn-Teller distortions are shown to have a small effect on the system due to the relative rigidity of the σ skeleton. The energy of vacancy formation as well as the energy of atom displacement and vacancy migration are directly computed from the change in total lattice energy, the results being in good agreement with experiment. The importance of introducing charge self-consistency in treating the charge redistribution in the system as well as the significance of allowing more distant atoms to interact with the vacancy electrons, is emphasized.

I. INTRODUCTION

The understanding of the electronic properties of point defects in graphite is of substantial practical and theoretical interest. From a practical point of view, the investigation of the elementary defects (vacancy, Frenkel pair) in graphite seems to furnish an essential initial step towards the understanding of the macroscopic phenomena associated with radiation damage in nuclear graphite (e.g., mechanical deformation of the lattice,[1-3] release of stored energy,[4] changes in conductivity,[5,6] etc.). Theoretically, the study of deep defect levels in covalent solids may be conveniently performed by reference to graphite. The theoretical framework underlying the calculations for defects and for the regular lattice, can be checked by comparison with the large amount of experimental information (noted in the introduction to paper I) pertaining to both situations. Of particular value would be to utilize the data on the extended crystal properties characterizing the regular lattice and on localized properties associated with deep defect, so as to correlate the eigenvalue spectrum and the charge densities of both systems. Thus, in the present paper we extend our study on the regular lattice (previous paper) to the investigation of point defects in graphite. Using a charge self-consistent LCAO (linear combination of atomic orbitals) scheme and a large basic unit cell (≤ 50 atoms) with the defect placed at its center, we investigate the one-electron spectrum associated with the defect, density of states, charge distribution, and the role of lattice relaxations around the defect, in a way similar to that previously employed to treat the regular lattice using the primitive unit cell (two atoms) representation.

II. NATURE OF THE PROBLEM

In view of the experimentally known characteristics of deep defect levels in covalent solids, the following considerations should be borne in mind before any theoretical approach is undertaken.

(i) Experimental studies on vacancies in covalent solids have shown that the wave function associated with the defect state is not amenable to description by either of the two limiting outlooks; namely, the complete localization of the wave function in the vicinity of the defect site (as used in the description of F centers in ionic crystals[7]) or the extended diffused model (used in the description of shallow impurity states in semiconducting covalent solids[8]). In fact, EPR (electron paramagnetic resonance) and NQR (nuclear quadrupole resonance) data on point defects in covalent

systems, suggest[9-11] that roughly 50 to 70% of the defects wave function is localized in a "sphere" surrounding the defect and its nearest neighbors, the remaining tail of the wave function extending onto more distant atoms.

This has a twofold implication: in terms of the theories using the band structure of the regular lattice for construction of the perturbed states (either by the Slater–Koster[12,13] or by direct expansion methods[14]) this suggests that a substantial part of the Brillouin zone (BZ) and more than a single electronic band should be taken into account for constructing the proper defect states. In terms of theories using a direct-space representation in treating the defect and its nearest neighbors (as the "defect molecule"[15,16]), this implies that more distant atoms could be important in determining the nature of the defect states. Methods belonging to the first class[12-14] become very difficult to implement in practice[13] when a large number of bands and points in the BZ are to be included, and have been shown[17] to reveal remarkable sensitivity to the choice of the grid points in the reciprocal space when a limited number of high-symmetry points is used, to the number of bands that are allowed to interact and to the number of neighboring atoms that are included in the defect's interaction range. Extensions to the original "defect molecule" approach, on the other hand, based on treating larger clusters of atoms in a truncated crystal approach,[18,19] do not provide a satisfactory correlative scheme between the defect levels and the edges of the crystal bands and reveal an artificial charge inhomogeneity inside the cluster owing to the presence of a large number of "dangling" bonds on the surface. Also, effective-mass approaches,[8] become ineffectual when the short-range part of the potential contributes significantly to the total interaction.

(ii) The formation of a vacancy in covalent solids and the accompanying bond breaking have been shown[11,18] to induce a substantial charge redistribution around the defect site. Thus, the mean field experienced by the defect electrons can no longer be approximated by the charge density obtained from the *perfect crystal* eigenvectors and one has to introduce self-consistency in order to modify the unperturbed interaction potential and the eigenvectors associated with the bulk of the crystal. In the direct-expansion methods based on pseudopotential formalism,[20] the charge-redistribution effects are partially accounted for by phenomenologically introducing various forms of screening in the local defect pseudopotential, while in the defect molecule approaches one estimates the effects of charge redistribution by using as basis orbitals different trial functions corresponding to various assumed hybridizations,[21,22] or by adding a semiclassical polarization term obtained from the static dielectric constant, to the calculated defect molecule energy.[23,24] Truncated-crystal models are not amenable to a direct self-consistent treatment since, owing to the surface effects involved, the iteration cycle would converge to the limit representing the bare cluster and not the defect in the infinite crystal. Simplified molecular models based on the linearization of the LCAO variational equations for the defect were able to achieve charge self-consistency;[25] however, its sensitivity to the rather drastic approximations involved is not yet clear. It should be mentioned that the introduction of charge self-consistency in the calculation necessitates the consideration of all the occupied levels in the solid and one cannot restrict the treatment to the defect levels alone or to assume a σ-π separation, etc., since the charge density needed for the readjustment of the crystal potential is determined by all states below the Fermi level. This observation excludes the use of simplified models using only a limited subset of the crystals eigenfunctions (e.g., π-orbital methods) for treating self-consistently defect problems.

(iii) Lattice relaxations around the vacant site were shown to induce large changes in the electronic properties of deep defect levels.[26,27] The forces exerted by the vacancy on the rest of the crystal lead to substantial relaxations of high-symmetry type, and in cases of a degenerate ground state also to Jahn-Teller distortions with typical relaxation energies of the order of 0.5–2 eV.[18,26,28] Treatment of such effects by perturbative methods using the perfect-crystal eigenvector as zero-order functions[12-14] is difficult owing to the enhancement of the perturbative potential associated with relaxed defects. Simple defect-molecule models[15,16] are obviously unable to reproduce a reasonable lattice-response function although in later elaborations[29,30] the influence of the crystal elastic behavior was introduced by attaching *equilibrium* force constants to the defect molecule. Besides the fact that such treatments include an additional assumption on the adequacy of the central-force model, it is not clear whether the inclusion of an *equilibrium* response taken over from the regular crystal data both in valence-force models[31-33] and in extended defect-molecule models[29,30] represents adequately the restoring forces in the presence of a vacancy.

In the present paper we present calculations on the point vacancy in graphite based on the small-periodic-cluster (SPC) model[34-37] in which one can treat the problems of localization, charge

self-consistency, and lattice relaxation in a straightforward manner. The method is based on the representation of the defect eigenvalue spectrum by the one-electron energies of a *periodic* array of atoms with the defect placed in its center. A self-consistent LCAO scheme is used and the interaction between all crystal bands and an effectively large number of points in reciprocal space is considered through the use of the recently developed mean-$\vec{k}$-points theorems in the BZ.[38,39] Problems regarding the undesired defect–defect interaction in the present defect-superlattice model as well as the role of many-electron effects, are discussed. The use of a calculation scheme similar to that employed for treating the electronic properties of the regular lattice of graphite (paper I, hereafter referred to as I) enables us both to correlate the electronic properties of the vacancy with that of the perfect lattice and to examine the adequacy of the theoretical description used by comparing the calculated results with the large amount of data existing on regular and vacancy-containing graphite.

III. METHOD OF CALCULATION

In the self-consistent band calculation on the perfect graphite crystal (I), we have considered a basic primitive cell of area a^2 (where a is the lattice constant) containing $h=2$ atoms. σ atomic orbitals were placed on each site and the self-consistent solution of the $\sigma h \times \sigma h$ variational equations defined the expansion coefficients $C^{\alpha}_{\mu j}(\vec{K})$ of the crystal functions j in terms of the basis Bloch orbitals, where $\mu = 1, \ldots, \sigma$, $\alpha = 1, \ldots, h$, and $j = 1, \ldots, \sigma h$. The wave vector $\vec{K}$ was restricted to the primitive BZ of area a^{-2} and at each iteration stage, the charge density was recomputed on a basis of the expansion coefficients $C^{\alpha}_{\mu j}(\vec{K}_\lambda)$ of the occupied bands, calculated at a selected grid $\{\vec{K}_\lambda\}$ in this primitive Brillouin zone (PBZ). If one were to repeat the calculation by using, instead of a *primitive* basic cell, a larger cell containing p and q primitive cells along the two crystal directions, respectively (a cell of area pqa^2, containing pqh atoms) one would obtain the same band structure where the new $pqh\sigma$ bands will be defined now in a small Brillouin zone (SBZ) characterized by wave vectors $\vec{k}_i$. Any point $\vec{k}_i$ in the SBZ would correspond to a discrete set of pq points $\vec{K}_l$ in the PZB (by folding in the PBZ). The distribution of the points $\vec{K}_l$, $l = 1, \ldots, pq$ corresponding to a given $\vec{k}_i$ point in the SBZ, depends on the p and q alone and can be easily obtained for every space group. Table I demonstrates the distribution of the $\vec{K}_l$ points associated with $\vec{k}_i = 0$ (Γ point) for the two-dimensional graphite structure where

TABLE I. Number of points in the primitive Brillouin zone which correspond to the $k_i \equiv \Gamma$ point in the small Brillouin zone, built up from clusters containing $p \times p$ primitive unit cells. Γ— BZ center, P— BZ corner, Q—center of the BZ edge (see Fig. 1, paper I), T—ΓQ line, S— ΓP line, I denotes an integer.

Number of points	Type
1	Γ
$3\delta(p/2)$	Q
$2\delta(p/2, I)$	P
$3[(p-1)-\delta(p/2, I)]$	T
$2[p/3-\delta(p/3, I)]$	S
$\propto p^2$	general point

$p = q$ (and hence the unit cell has the area p^2a^2). It is observed that the solution of the variational equations at the hexagonal zone center, based on a unit cell of lengths pa, always yields the Γ point, a maximal degeneracy of three and two for the high-symmetry points Q and P in the primitive BZ representation, respectively (see Fig. 1, paper I for notations) while the number of general points yielded *increases as* p^2. Similar correlations tables may be easily obtained for any other point in the small BZ. One can now calculate the charge density required in the self-consistency procedure, by replacing the sum over the PBZ:

$$\rho(\vec{r}) = \sum_{\vec{K}}^{\mathrm{PBZ}} \sum_{\mu,\nu} \sum_{\alpha,\beta} \sum_{j} C^{\alpha}_{\mu j}{}^{*}(\vec{K},\vec{r})\, C^{\beta}_{\nu j}(\vec{K},\vec{r}) \times \Phi^{\alpha}_{\mu}{}^{*}(\vec{K},\vec{r})\Phi^{\beta}_{\nu}(\vec{K},\vec{r}), \qquad (1)$$

by the sum of $\vec{k}_i$ over the SBZ (each of them corresponding to p^2 vectors in the PBZ and carrying a weight proportional to the relative volume it occupies). The lowest approximation to this will be to use only the Γ point in the SBZ.

This represents only a minor complication over the common quantum-chemical approach toward the self-consistent LCAO solutions for polyatomic molecules and provides directly information on electronic properties of periodic solids. This problem has been previously treated by one of us for graphite,[35,36] boron nitride,[34] and hydrogen fluoride.[37]

Higher approximations to the fully self-consistent solutions would be obtained by including the eigenvalues corresponding to several $\vec{k}_i$ points in the SBZ. The best choice of a limited set of $\vec{k}_i$ points would be obtained by applying the mean-value theorem in the BZ of Chadi and Cohen[38] and Cunningham[39] to the *small* BZ. The set of points generated by this algorithm comprises the best limited selection of points needed in calculating averages of periodic functions over a given BZ. Since a given $\vec{k}_i$ point in the small BZ al-

ready yields a distribution of p^2-$\vec{K}_i$ points with weights proportional to the volume they occupy in the BZ, selection of several such $\vec{k}_i$ points according to the mean value theorem should furnish a good verisimilitude to the totality of points in the BZ. The accuracy of the average of an expectation value calculated from the mean value points is determined by the smoothness of the bands. Owing to the substantial lowering of the dispersion of the original bands in the small BZ representation, this accuracy improves. One can thus set a complete self-consistent calculation on a perfect solid by defining a large unit cell and solving for Bloch type states in that system using a small number of well-chosen eigenvectors to obtain the ground-state charge density at each iteration. Since the number of general $\vec{K}$ points projected into a single $\vec{k}$ point in the SBZ increases rapidly with unit cell size (e.g., Table I), one might also hope to obtain accurate estimates of properties determined by averaging over the BZ, such as the total energy per atom, elastic constants, etc., by using a few $\vec{k}$ point representations.

This small-periodic-cluster (SPC) scheme is obviously inefficient when one is interested in *perfect* periodic systems, (since the large $p^2h\sigma \times p^2h\sigma$ secular equations can be evidently block diagonalized to p^2 equations of order $h\sigma \times h\sigma$ using the translational invariance in the primitive unit-cell basis.) We are using it in effect only for defect problems, where this type of translational invariance does not exist. This is simply done by repeating the solution of the eigenvalue problem in the SPC representation *after replacing a host atom in the large unit cell by a vacancy*. The self-consistent solution of the Bloch problem in a vacancy containing large unit cell ($p^2h - 1$ atoms), corresponds to a periodic-defect-superlattice solution. One then approaches the limit of non-interacting point defects simply by increasing p. Although there are some interesting aspects in the interacting defect superlattice limit itself,[37,40,41] we will be interested in this paper solely in the *point* defect problem. The superlattice representation does not place a severe restriction in studying deep defect states in covalent systems since the localization radius is usually well below 2–3 lattice constants. In any case, the residual defect–defect interaction present in our model will be directly evaluated by using the dispersion of the defect band and the calculated range of the perturbative defect potential as monitors to such residual interactions.

The defect–defect interaction consisting of a direct electrostatic effect and the force-multipoles displacement field effect[42] has been shown to decay with the defect–defect distance R as R^{-5} and R^{-7},[42,43] respectively. Furthermore, in hexagonal systems like graphite and boron nitride exhibiting a large anisotropy, the vacancy–vacancy interaction in the basal plane is slightly attractive and much reduced relative to the interaction of defects parallel to the c axis.[43] Thus, the direct vacancy-vacancy interaction in the basal plane of graphite is expected to be rather small and to decay very fast with increasing separation and hence the defect superlattice representation should not place any severe limitation when applied to such systems.

The main advantages of the proposed SPC model in studying defect problems are:

(i) Both resonating and localized states are directly obtained from a single variational solution. This should be contrasted with some t-matrix formulations and simple resolvent schemes[12,13] that concentrate only on one type of solution.

(ii) The edges of the perfect crystal bands (conduction edge, valence edge, separation between unperturbed valence bands, etc.) are completely defined in the problem. The separation between defect levels and the crystal bands can thus be directly compared with experiment without the need of invoking the correct band-edge location from a separate calculation, as is often the case in cluster models.[18,19]

(iii) The degree of localization of the defect states is not preassumed (as is the case in applying effective-mass theories to nonshallow defects) but rather comes out naturally from the calculated eigenvectors.

(iv) The defect perturbative potential is not transferred from unperturbed crystal data (as done in the pseudopotential treatment of point defects[20]) but is calculated self-consistently from the charge density obtained in a variational LCAO solution in which the basis orbitals situated on the vacant site are removed. The separate self-consistent solutions on the perfect and defected system enable one to calculate the perturbative defect potential simply by subtracting the two self-consistent potentials (see below).

(v) Owing to the periodic boundary conditions placed on the system containing large unit cells, no unrealistic charge redistribution or surface states are present, as is the case in cluster models.[18,19]

(vi) An effectively large number of unperturbed crystal states and atomic neighbors are allowed to interact in forming the defect eigenstates. This should be contrasted with the defect molecule models treating only nearest-neighbor interactions or with simple few-bands Slater-Koster models.[12]

The main disadvantages of the present SPC model are:

(a) The large number of interacting states in the model result in large dimensions ($p^2h\sigma \times p^2h\sigma$) of the secular equations (each element being a lattice sum in itself) to be solved. This forced us to restore to rather simplified LCAO algorithms (the modified iterative extended Hückel) for calculating the matrix elements. This is certainly an undesirable feature of the present treatment. However, as demonstrated in the previous paper (I), a judicious choice of the LCAO scheme, using only a few parameters taken over from essentially *atomic* (and not solid-state) data, is capable of revealing excellent agreement between experimental and calculated optical interband transition energies, photoelectron spectroscopy (ESCA) data, secondary-electron-emission data, Fermi-surface characteristics, bond lengths, and binding energy in the perfect system.

(b) Owing to the defect superlattice representation in the SPC model, large unit cells should be employed in order to reach the limit of weakly interacting defects. This restricts presently the use of the method to systems exhibiting a localization range smaller than two to three lattice constants. Most color-center problems in alkali-halides and deep defects in semiconducting and insulating covalent systems fall within the range of applicability of this method.

IV. RESULTS

A. Unrelaxed vacancy

The energy eigenvalue spectrum associated with a point vacancy is obtained by solving self-consistently the coupled LCAO equations [Eqs. (1)–(4) in paper I] for a crystal whose basic unit cell is composed of p^2 primitive cells, with a vacancy at its center. The basic cell contains $2p^2 - 1$ atoms where p runs over the values 2–5 (so that there are clusters of 7, 17, 31, and 49 atoms, denoted C_7V, $C_{17}V$, $C_{31}V$ and $C_{49}V$, respectively) and the separation between two nearest defects in the superlattice is pa, where a is the primitive lattice constant. On each carbon atom a minimal valence basis of $2s$, $2p_x$, $2p_y$, and $2p_z$ Slater orbitals are used with standard Slater exponents. Self-consistency is obtained by recalculating the charge density matrix and the net atomic charges at each iteration step, on the basis of the eigenvectors belonging to all bands below the Fermi energy at a discrete set of $6p^2$ or $3p^2$ $\vec{K}$-points. These sets of points in the Brillouin zone are generated by applying the mean value theorem of Cunningham[39] to the *small* BZ using his $6\vec{k}$ and $3\vec{k}$ sets, respectively. The self-consistency criterion is set at 1×10^{-3} e for the charge-density elements and 10^{-4} eV for the one-electron energies. The matrix elements in the atomic basis set [Eq. (4) paper I] are evaluated within the modified extended Hückel approximation employing the same parameters that have been used in paper I to discuss the regular lattice. The limit of noninteracting defects is sought by increasing the value of p (and hence the defect–defect distance) and using the degree of dispersion of the defect band and the perturbations in the electrostatic potential associated with it (via the solution of the appropriate Poisson equation) as monitors to the residual defect–defect interaction.

The spread of the energy bands obtained by sampling a single $\vec{k}$ point (i.e., $\vec{k} = \Gamma$) in the small BZ for the unrelaxed lattice is depicted in Fig. 1(a). As the size of the large unit cell increases, more states are sampled by the Γ point in the small BZ (see Table I) and the band pattern (widths of bands, σ-π overlap, etc.) converges to a constant limit. Since the vacancy containing lattice still possesses the basal plane σ_h reflection symmetry, its eigenvectors are partitioned into pure π type and σ type levels in exactly the same man-

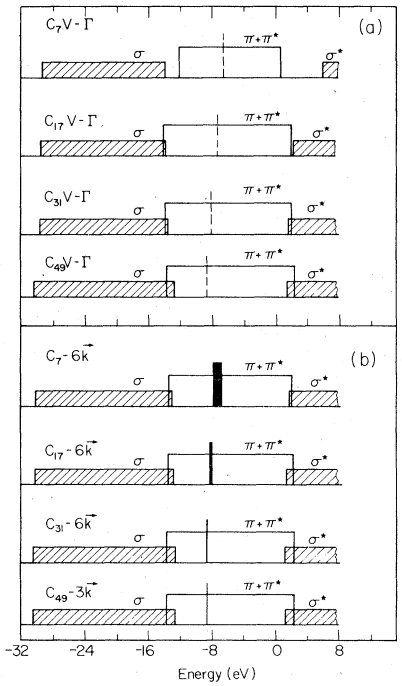

FIG. 1. General pattern of the eigenvalue spectra of an unrelaxed vacancy in graphite as obtained from the calculations including the (a) Γ—point in the small BZ for all clusters. The dotted line indicates the position of the defect level. (b) Six special points for C_7V, $C_{17}V$, and $C_{31}V$ and the three special points for the $C_{49}V$ cluster. The dark area in the $\pi - \pi^*$ region denotes the position of the defect levels, while the dashed areas label the σ and σ^* bands.

ner as in the regular lattice. A doubly degenerate σ level of e' symmetry in the local D_{3h} point group is observed to peel off the valence band and appears in the pure π region located in the σ-σ^* band gap. This level is spatially localized on the atoms surrounding the vacant site and constitutes a localized defect gap state. Assignment of $(2p^2-1)$ and $3(2p^2-1)$ electrons to the π and σ levels, respectively[21] leaves this defect σ level singly occupied in the ground state of the neutral vacancy system. The defect structure as a whole still possesses one π electron and three σ electrons per carbon atom as is the case in the unperturbed lattice. Thus, although graphite is a semimetal with zero band gap (owing to the degeneracy of the π valence and conduction bands at the hexagonal BZ corner) it exhibits true localized σ gap states upon vacancy formation since it is actually a high gap insulator in its σ manifold. It is seen from Fig. 1(a) that sampling of the Γ point alone in the small BZ is insufficient to account for the limiting shape of the bands when the relatively small (C_7V, $C_{17}V$) clusters are considered. Furthermore, only a small number of translational representations (four and nine, respectively) are allowed to interact in forming the defect level. Sampling now the six special $\vec{k}$ points[39] for the C_7V, $C_{17}V$, and $C_{31}V$ clusters (i.e. 24, 54, and 96 $\vec{K}$ points in the primitive BZ) and the three special $\vec{k}$ points for the $C_{49}V$ cluster (i.e., 75 $\vec{K}$ points), one obtains [Fig. 1(b)] a stabilized band pattern and a broadening of the defect level into a defect band. The variation in the characteristic of the σ defect band reflects now only the defect–defect interaction present in the superlattice representation. We now seek the limit of noninteracting defects by examining the convergence of the various features of the defect band as a function of the cluster's size. It should be emphasized that a similar convergence check performed on the properties of the defect band when only a single $\vec{k}$ point is sampled in a small cluster,[18] does not necessarily reflect the suppression of the defect–defect interaction but rather the combined effect of allowing more $\vec{K}$ representations to interact and the increase in the defect–defect separation. Figure 2 shows, as a function of cluster size the convergence of the energetic position of the center of the defect band with respect to the valence-band edge, the width of the defect band, and its degree of spatial localization. The last quantity is defined as the percent of electronic charge in the defect band alone, residing on the three nearest-neighbor atoms [where the charge definition is that discussed in paper I, Eq. (A8)]. It is observed that the defect–defect interaction is effectively suppressed in the $C_{31}V$ and $C_{49}V$ clusters as can be judged from the vanishing dispersion of the defect band, the stabilization of its energetic position and the leveling off its degree of localization.

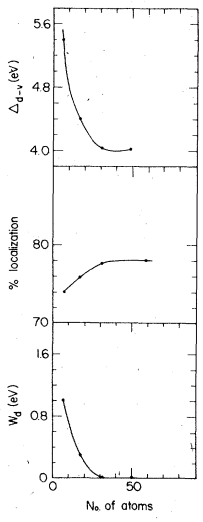

FIG. 2. Convergence of the energetic separation of the center of the defect band from the valence σ band (Δ_{d-v}), the percent localization of the defect band and its width (W_d) as a function of cluster size. Six special $\vec{k}$ points are used for C_7V, $C_{17}V$, and $C_{31}V$ and three special $\vec{k}$ points are used for the $C_{49}V$ cluster.

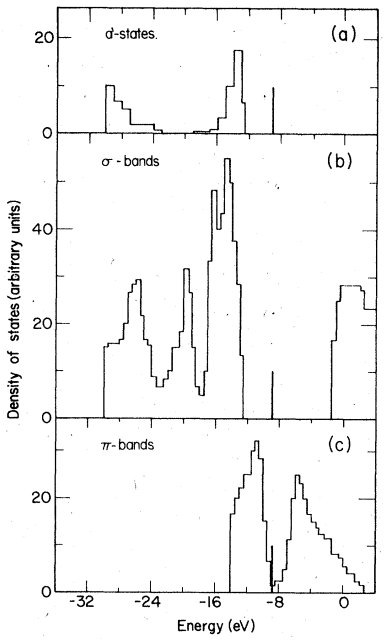

FIG. 3. Partial density of states of the lattice with an unrelaxed vacancy as obtained by sampling the six $\vec{k}$ points in the $C_{49}V$ cluster. Histogram box width: 0.5 eV. (a) a' levels in the occupied σ bands. (b) σ bands. (c) π bands. The full line in the σ-σ^* gap indicates the position of the defect level.

Figure 3 shows the partial density of states of the solid containing an unrelaxed vacancy, as obtained by sampling the six special $\vec{k}$ points in the $C_{49}V$ cluster. The general pattern of the density of states is similar to that obtained for the regular lattice (Fig. 5, paper I) except for the occurrence of the defect level in the σ-σ^* gap. In addi-

tion to this highly localized σ defect level, the valence σ band contains an entire distribution of resonant states of a' symmetry with degrees of localization varying around 20–30%. The partial density of states of these levels is depicted in Fig. 3(a) and is seen to peak near the band edges. In the absence of a lattice distortion that would remove the degeneracy of the π bands at the BZ corner, no real localization could be found in the π system and their dynamic response should be describable by scattering of the metallic π Bloch waves by the defect.[44]

The variation in the density of states of the delocalized π system due to defects, has been considered by Boardman *et al.*[45] using a Green's-function formalism in the Wannier representation and the one-site approximation to the perturbing matrix elements with the neglect of interband coupling terms. This has suggested a very small change (of ~1%) in the density of π states near the Fermi level, for low defect concentration. Although the π system undergoes minor modifications upon introducing a small number of defects, it manifests, however, an important indirect effect on the σ localized defect levels through the changes induced in the total $\pi+\sigma$ electronic charge that determines the coupling matrix elements. This effect will be discussed below.

It is interesting to compare the electronic structure of the neutral vacancy obtained here with that yielded by the defect molecule approach of Coulson *et al.*[21] In the latter model the vacancy structure is represented by three σ-type sp^2 dangling orbitals centered on the three atoms surrounding the vacant site. Linear combinations of these three orbitals are built up according to the a' and e' irreducible representation of the D_{3h} local point group. In the neutral vacancy, three electrons are available for these levels while the rest of the six σ electrons and the three π electrons are considered to populate the three sp^2 orbitals pointing away from the vacancy and the three perpendicular π orbitals, respectively, and are not considered explicitly. The three σ electrons give rise to the a'^2e' configuration (associated with the $^2E'$ many-electron state) and to the $a'e'^2$ configuration (associated with the many-electron terms $^2A_1'+{}^4A_2'+{}^2E'$). The degree of localization in each of the one-electron molecular orbitals is assumed to be 100% (neglecting all except the first-nearest neighbors) and lattice relaxations are ignored. The coupling with the electronic states of the bulk crystal is similarly neglected. The two many-electron terms $^2E'$ arising from the a'^2e' and $a'e'^2$ electronic configurations are then allowed to interact through a semiempirical configuration-interaction treatment resulting in a very small admixture between them due to the large separation (6–8 eV) between the zero-order e' and a' levels. The ground state of the neutral vacancy is then unequivocally assigned to the $^2E'$ state arising from the a'^2e' configuration.

In the treatment of the neutral vacancy presented in this paper, many-electron effects are explicitly neglected. The vacancy orbitals are allowed to couple with the crystal eigenstates and an interaction range of 2^2-1 to 5^2-1 neighboring primitive cells is considered in a self-consistent treatment using 24–96 representative $\vec{K}$ points in the BZ. This results in a *manifold of resonant a' levels lying inside the valence band* (instead of a single, completely localized a' level carrying two vacancy electrons in the defect molecule model) and in a singly occupied e' level, being pushed out of the band. Using the notation of the defect molecule model, the resulting configuration might be denoted as $\{a_i'^2;\ i=1,\ldots,N\}e'$. Owing to mixing with the crystal-band states of similar symmetry, the $\{a'\}$ states are substantially delocalized in the solid and reveal an energy spread throughout the σ valence band [Fig. 3(a)]. Owing to the neglect of all but the three-nearest-neighbor atoms in the defect molecule model, one is forced to assume a completely localized a' level carrying the vacancy electrons. Several conclusions can be drawn from this comparison:

(i) Many-electron effects could have been treated on the basis of the e' configuration for the ground state rather than the a'^2e' configuration, resulting in a much simpler treatment. This stems from the fact that the a' orbitals seem to form a part of the closed-shell valence band.

(ii) Many-electron correlation effects resulting from the coupling of the ground state with higher terms, that have been shown to be rather small in the original defect-molecule work (a few tenth of an eV) would be even reduced when one would use the appropriately delocalized a' crystal orbitals instead of the highly localized orbital used in the defect molecule work. (This results from the fact that the integral over the distribution of the delocalized a' levels of the square of the perturbative two-electron matrix elements is smaller than the square of the corresponding matrix element evaluated for a peaked distribution.) Thus, unlike the situation present in defects in other covalent systems (vacancy in diamond[15,16] and silicon[29]), many-electron effects are probably very small for the neutral vacancy state in graphite and the one-electron LCAO description can be safely adopted. A similar decrease of many-electron correlation effects owing to increase of the delocalization space available for the defects electrons has been suggested by Watkins and Messmer[18(c)] on the basis

of a spin unrestricted $X\alpha$ cluster calculation for a vacancy in diamond. The situation met in graphite is, however, much simpler, as discussed here, owing to the single occupancy of the defect orbital and the overlap of the a' levels with the occupied bands.

(iii) One-electron properties, as revealed by the defect molecule model, can be roughly correlated with those yielded by the present model, by considering *average quantities*. Thus, in Coulson's model the a' level lies some 6–8 eV below the e' level while the SPC results show that the center of the highest peak in the $\{a'\}$ density of states lies some 5 eV below the e' level. The lowest optical transition in the defect molecule model occurs between the $^2E'$ and the $^2A_1'$ states at 5–7.7 eV (depending on the values of the empirical integrals involved). The transition from the ground state to the center of gravity of the excited states arising from the $a'e'^2$ configurations occurs at about 4–6 eV, compared with the corresponding one-electron transition energy in our model of 5 eV. It should, however, be noted that while the lowest transitions in the defect molecule model occur between spatially localized configurations, the SPC model reveals in addition a transition of lower energy (4.0 in the unrelaxed lattice) from the top of the valence band [Fig. 3(b)] to the localized e' band.

We briefly summarize now the changes introduced in the calculated electronic structure of the defect system due to maintenance of self-consistency in our calculations.[46] Figure 4 shows the partial π and σ charges (Q_π and Q_σ) and the net atomic charge ($q_{\rm net}$) on one of the nearest-neighbor atoms to the defect site as a function of the self-consistent iteration cycle number. It is seen that the substantial charge accumulated on the nearest-neighbor atom in the uniterated results ($q_{\rm net} = 0.85e$) is strongly reduced (up to $0.16e$) upon reaching the convergence limit. The main redistribution effects occur in the π system while the variation in σ charge is smaller. Thus, as a result of the vacancy formation the π electrons tend to avoid the vacant site and accumulate on the nearest-neighbor atoms (loosing thereby some π delocalization energy), unlike the situation in shallow impurities in semiconductors and in F centers in ionic solids.[7,8] The accumulation of excess π charge on the carbon–carbon bonds surrounding the defect (as manifested also by an increase of 23% in the π bond order of these bonds), is liable to increase the stability of these bonds relative to the normal c-c bonds in graphite and thereby induce symmetric lattice distortions. This possibility will be discussed in Sec. IV B together with the Jahn-Teller distortions. The atoms that are next-nearest neighbors to the defect reveal only minor ($10^{-2}e$) charge perturbations. (It is noted that in the present study we have chosen not to utilize the symmetry of the eigenvectors to reduce the size of the secular equations,[47] partially because of the need to consider the full-charge density matrix in the self-consistent treatment and because lattice distortions of arbitrary symmetry are to be discussed.[48])

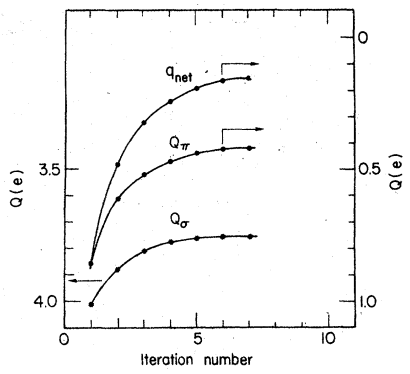

FIG. 4. Variation in the π charge (Q_π), σ charge (Q_σ), and net charge ($q_{\rm net}$) on an atom that is a nearest neighbor to the vacancy, during the self-consistent iteration cycle.

Through the self-consistent iteration history,[49–52] the defect level undergoes a destabilization from −10.30 to −8.6 eV, thus approaching the low density of states region near the Fermi level, characterized by a fairly steep slope (Fig. 3). The occurrence of a localized vacancy acceptor state at the vicinity of the Fermi level, as obtained here, is in accord with the common concepts on electron trapping mechanisms in irradiated graphite.[53] Thus, in addition to the small modification[45] in the mobile π electron density near the Fermi level due to defect formation, the occurrence of localized states at this energy is consistent with the behavior of the Hall coefficient,[54,55] the electron-spin resonance,[56,57] and the diamagnetic susceptibility.[58,59] The initial sharp increase of the Hall coefficient for low irradiation dose has been attributed to removal of electrons by trapping[54,55] and the decrease in the thermoelectric power with increasing exposure was argued[53] to arise from an increase in the hole concentration due to localization of electrons in acceptor states. The increase of diamagnetism with bombardment[58] and the reduction in the EPR g factor[56,57] have been similarly discussed in terms of trapping mechanisms.

The decrease in the energy of the defect level upon iterating towards self-consistency, is accompanied by a stabilization of the total cluster

energy by 1.8 eV and by an increase in the degree of localization of the defect level, from 78 to 86%. The stabilization of the total energy arises from the charge rearrangement in the nonlocalized band states.[60] The increase in the localization of the defect wave function makes it easier to approach the limit of uninteracting defects in our superlattice model when the system is treated self-consistently. Self-consistency effects are thus of considerable importance even in the homonuclear systems and cannot be neglected.[18,19] Similar conclusions on the importance of self-consistency and screening effects in defect calculations have been previously emphasized by several authors.[25,61,62]

The energy required to separate a carbon atom from the cluster and to bring it to infinity in its ground atomic configuration (vacancy self-energy, E_v) was calculated from

$$E_v = E_{\rm tot}(N) - [E_{\rm tot}(N-1) + E_{\rm tot}(1) + E_{\rm pro}] , \quad (2)$$

where $E_{\rm tot}(M)$ denotes the total energy of all the occupied states of a cluster containing M atoms and $E_{\rm pro}$ denotes the promotion energy from the valence sp^2 state to the ground atomic ^3P configuration. $E_{\rm tot}(N)$ and $E_{\rm tot}(N-1)$ were calculated by sampling the six special points in the $C_{32}-C_{31}V$ and $C_{50}-C_{49}V$ clusters and the promotion energy was taken from the theoretical results of Goldfarb and Jaffe.[63] At this level of approximation, $E_{\rm tot}(N)$ is minimized with respect to the perfect-crystal unit-cell parameter (yielding $a_{\rm min}=2.482$ Å compared with the experimental value $a=2.46$ Å,) but $E_{\rm tot}(N-1)$ is not minimized with respect to relaxations of the lattice atoms around the vacancy site. In this static approximation we obtained $E_v=12.56$ and 12.61 eV for $C_{31}V$ and $C_{49}V$, respectively. The energy of vacancy formation $E_{\rm vf}$ in the unrelaxed lattice is given by subtracting from this the sublimation energy E_s gained by the system when the ejected atom is adsorbed on the crystal surface. Using the experimental value[64] $E_s=7.40$ eV for the sublimation energy, one obtains $E_{\rm vf}=5.2$ eV. Comparison with experiment will be discussed in Sec. IV B where relaxation corrections will be introduced. In our previous calculation on vacancy formation[35] a value of $E_{\rm vf}=3.0$ eV was obtained where only the $\vec{k}=0$ point was sampled and the $C_{17}V$ and $C_{31}V$ clusters were used in a simple iterative-extended-Hückel calculation, using slightly different atomic parameter. The loss of π energy alone upon vacancy formation is calculated here to be 2.1 eV. This is smaller than the π energy per atom in the regular lattice (part I) signifying that the rearrangement in the electronic structure accompanying vacancy formation serves to recover a part of the loss in the π delocalization energy.

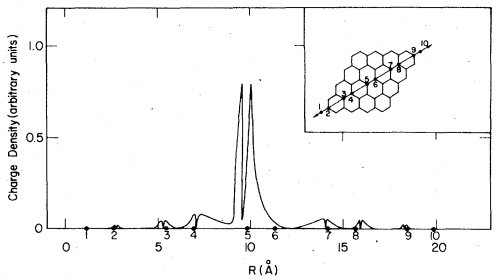

FIG. 5. Charge density of the defect level along the line indicated in the inset. The numbers at the lower part of the figure correspond to the numbering of atoms in the inset, where site No. 6 indicates the vacancy site. Only sites 5 and 6 along the indicated line are considered in a simple "defect-molecule" model.

In addition to the energetic characteristics associated with the defect (defect level, density of states, etc.) of considerable interest are also the spatial behavior of the charge density and the electrostatic potential introduced by the vacancy. Figure 5 shows the charge density of the defect level along the line shown in the insert to that figure. Most of the density is shown to be localized on the nearest-neighbor atom (denoted in Fig. 5 as site 5) and on the aromatic hexagonal ring following this atom (the 5–4 region in Fig. 5), however, non-negligible charge resides also on more distant atoms. The charge density of the defect band has about 10% of $2s$ character, the rest being of $2p_x$ and $2p_y$ character. This admixture is manifested by the shift of the characteristic node of the $2p$ orbitals away from the atomic sites. Thus not only the uppermost σ valence band (σ_3 in the notation of paper I) is contributing to the defect level (the latter being a pure $2p$ band, see Fig. 6 in part I) but also the lower σ_1 and σ_2 bands. This demonstrates the inherent difficulties associated with theoretical models on the vacancy problem in covalent solids—a nearest-neighbor defect molecule model would significantly reduce the delocalization space available for the vacancy electrons (only sites 5 and 6 in Fig. 5 are considered by such models) while a simple truncated-crystal model involving a similar number of atoms as the SPC model is liable to distort the wings of the defects wave function due to the penetration of surface effects associated with the dangling bonds. Simple one-band Slater-Koster type models, on the other hand, are incapable of revealing the extensive band mixing exhibited by the present calculation. The need of more than a single energy band for the adequate description of the vacancy has been emphasized by Callaway.[13] The fact that the vacancy level emerges from the valence band and its wave

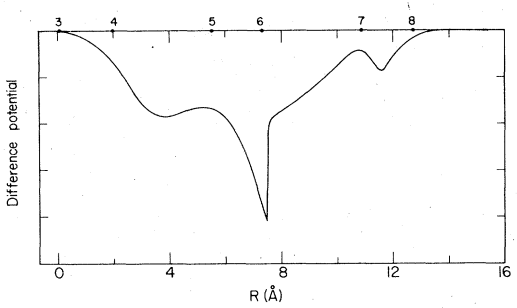

FIG. 6. Electrostatic potential difference (in arbitrary units) between perfect and vacancy-containing clusters, computed from the total valence density along the line shown in the insert to Fig. 5. Site 6 denotes the vacancy, upper numbering refers to Fig. 5.

function receives contributions mainly from the highest occupied σ valence bands, justifies the use of the extended-Hückel approximation for describing this state. In a previous paper (part I) it has been shown that the EXH approximation used here yields excellent agreement both with experimental data and with first-principles band calculations on the valence bands whereas the high conduction bands lying some 10 eV above the Fermi level are not properly described by this approximation.

Figure 6 shows the difference in the electronic electrostatic potentials between the perfect cluster and the one with a vacancy. The corresponding potentials are obtained from the solution of the Poisson equation by the method discussed in paper I [Eqs. (12) and (13)] where the charge density involved is calculated from all the occupied levels in the ground state. This potential is the self-consistent LCAO analog of the screened defect pseudopotential used in pseudopotential theory[14,20] and of the defect potential used in the linear Born approximation.[65] A rather rapid screening-out of the Coulomb potential is seen and this is accompanied by diffraction effects in the tails. The general behavior of the potential is similar to that obtained for a point charge in a Fermi gas[65] and to that anticipated from the Slater-Koster impurity model[44] but is markedly different from the smoothly decaying screened Coulomb potential obtained in the linear Hartree theory.[65] It should be stressed, however, that contrary to the defect potential derived from the simple Slater-Koster model, the self-consistent SPC defect potential reflects the contributions of *all perturbed valence bands* and not only that of a single band. The modification in the electrostatic potential due to the nonlocalized band states is important when one considers quantities that depend on the change in total crystal energy, such as energy of vacancy formation and migration.[61]

The difference potential shown in Fig. 6 and the defect charge density shown in Fig. 5 demonstrate that the perturbative effects associated with the vacancy are already very small after two or three primitive unit cells around the defect site. This implies that a periodic cluster representation based on 4×4 to 5×5 primitive cells (clusters $C_{31}V$ and $C_{49}V$, respectively) should furnish a reasonable model for treating this defect. The very small dispersion of the defect band obtained for clusters of this size, further support this conclusion.

Finally, we show in Fig. 7 the total valence electrostatic potential in the plane of the vacancy containing graphite lattice. It is seen that the region between the nearest neighbors and the next-nearest neighbors to the defect site is characterized by strong binding effects while a lower potential is revealed near the next-nearest neighbors themselves. A similar behavior was exhibited by the difference potential. As discussed above, charge redistribution effects tend to accumulate excess π charge on the bonds surrounding the defect. This would induce shortening of these bonds through lattice relaxation effects. Such effects are considered in Sec. IV B where relaxation effects are introduced.

B. Relaxed vacancy

The accumulation of excess charge on the bonds surrounding the vacancy site and the resulting build-up in the electrostatic potential, suggests that conformational changes might accompany the vacancy formation. Although the extended-Hückel total energy function [Eq. (10), paper I] constitutes only a rough approximation to the exact quantity,[19,66]

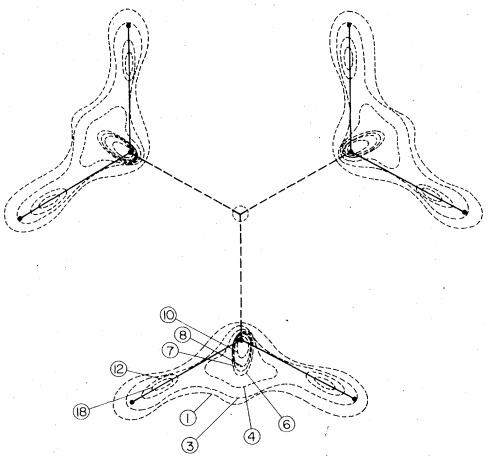

FIG. 7. Contours of the electrostatic potential of vacancy containing two-dimensional graphite in the layer plane. The numbering on the contours indicate relative heights.

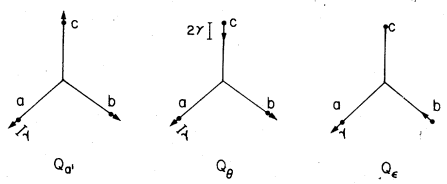

FIG. 8. Illustration of the three normal modes involved in local lattice relaxation around the vacancy in graphite.

the close agreement obtained between experimental and theoretical force constants for the regular graphite (see part I) and the elastic constants in diamond[18] suggest that this model could be used as a first approximation to estimate the restoring forces in the system. In this treatment we restrict ourselves to local deformation modes involving only the nearest-neighbor atoms to the defect site. In our defect-superlattice representation with 49 atoms, a next-nearest-neighbor relaxation would substantially increase the undesired defect–defect interactions. Relaxation studies on vacancies in other covalent solids, have indicated that the next-nearest-neighbor contribution to the formation energy is of the order 1–3%.[33, 67]

The three normalized normal modes belonging to the a' and e' representations of the local D_{3h} site symmetry (Fig. 8) are given by:

$$
\begin{aligned}
Q_{a'} &= (1/\sqrt{3})(-\tfrac{1}{2}\sqrt{3}\,X_a + \tfrac{1}{2}\sqrt{3}\,X_b - \tfrac{1}{2}Y_a - \tfrac{1}{2}Y_b + Y_c),\\
Q_\theta &= (1/\sqrt{6})(-\tfrac{1}{2}\sqrt{3}\,X_a - \tfrac{1}{2}\sqrt{3}\,X_b + \tfrac{1}{2}Y_a + \tfrac{1}{2}Y_b + 2Y_c), \qquad (3)\\
Q_\epsilon &= (1/\sqrt{2})(-\tfrac{1}{2}\sqrt{3}\,X_a - \tfrac{1}{2}\sqrt{3}\,X_b - \tfrac{1}{2}Y_a + \tfrac{1}{2}Y_b),
\end{aligned}
$$

where $(X_a Y_a)$, $(X_b Y_b)$, and $(X_c Y_c)$ denote displacement coordinates of atoms a, b, and c surrounding the vacancy and θ and ϵ are the two components belonging to the e' representation. The completely occupied valence band transforms according to the total symmetric a' representation, so the transformation properties of the total system are those of the singly occupied e' defect orbital. Distortions contained in the symmetric product $e' \times e'$ can result in splitting of the energy states. We thus distinguish between the symmetric distortion modes a' giving rise to a constant shift of the total and of the defect one-electron energies, on one hand, and the Jahn-Teller distortion e' giving rise to level splitting, on the other hand. For the sake of convenience the amplitude of distortion γ is defined as the decrease in the equilibrium nearest-neighbor vacancy-carbon bond length associated with a particular mode (Fig. 8). The $Q_{a'}$ and Q_θ distortion modes can be associated with either an inward ($\gamma > 0$) or an outward ($\gamma < 0$) relaxation while the Q_ϵ mode is invariant under the sign of γ. The carbon-carbon bond length for the unrelaxed lattice is taken as $R = 1.435$ Å corresponding to the equilibrium value obtained for perfect graphite in the extended Hückel calculation (part I). At this conformation the defect level appears at -8.4 instead of -8.6 eV. Local distortions belonging to the $Q_{a'}$, Q_θ, and Q_ϵ modes are thus applied with varying amplitudes γ and the change in the degree of localization of the defects wave function, the energetic shift of the defect level and the variation in the vacancy self-energy (defined as excess stabilization E_B over the unrelaxed value), are investigated. Owing to the complexity of a fully self-consistent treatment of the relaxation effect we have not attempted to reach convergence in the iteration cycle for each relaxed conformation but rather used the self-consistent results for the unrelaxed structure as standard input. The final relaxed conformation corresponding to the energy minima obtained (see below) was subjected to a self-consistent treatment resulting in relatively small modifications of the charge distribution. The minimization of the cluster's total energy with respect to the deformation coordinates is performed by the steepest-descent method [Eq. (11), paper I].

Figure 9 shows the degree of localization, the defects one-electron energy level position ϵ_d, and the excess binding energy E_B for the a' relaxation where positive values of γ correspond to shortening of the vacancy-carbon bond (and elongation of the bonds formed by the atoms a, b, and c with their nearest neighbors, see Fig. 10). It is seen that the vacancy self-energy reaches a minimum of -0.80 eV relative to the unrelaxed vacancy, at $\gamma = -0.065$ Å, corresponding to a decrease in each of the six bonds formed by atoms a, b, c with their nearest-neighbor carbons (denoted by open circles in Fig. 10) to 1.404 Å (-2.2% relative to the calculated equilibrium carbon-carbon distance in graphite) and to an increase of the three a-b, a-c, and b-c distances to 2.60 Å ($+4.8\%$ relative to the calculated value of the unperturbed lattice constant). The energy ϵ_d of the defect level passes through a minimum as a function of the a' distortion. The location of this minimum appears at a much smaller distortion amplitude than the corresponding minimum in the binding curve, suggesting that the stabilization of the fully occupied valence bands contributes more significantly to the lowering of the vacancy self-energy than the defect orbital itself. This is readily understood in terms of the different contributions from the π and σ systems to the relaxation energy. In the previous section we have shown that although the loss of π energy upon vacancy formation ($\Delta E_\pi = 2.1$ eV) constitutes a relatively small part of the total vacancy self-energy, the main charge redistribu-

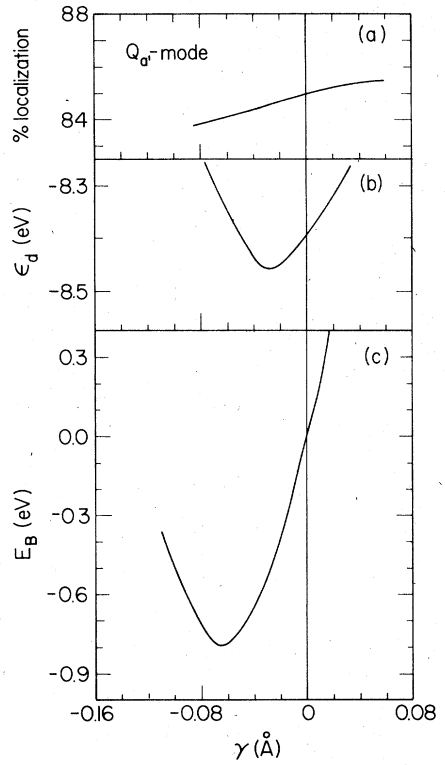

FIG. 9. Degree of localization of the defect wave function, energy (ϵ_d) of vacancy level, and the vacancy binding energy (E_B) (relative to the unrelaxed vacancy) obtained for the symmetric a' relaxation. Positive values of the changes in bond length, γ indicate inward relaxation.

tion effects accompanying the vacancy formation occur in the more polarizable π system rather than in the relatively rigid σ system. The relaxation induced bond shortening associated with the σ defect orbital alone [Fig. 9(b)] constitutes only a part of the total bond shortening that results from the stabilization of all occupied bands [Fig. 9(c)]. In fact, most of the stabilization gained by the a' relaxation comes from the π system that forms a part of the occupied valence bands. Though the system is loosing 2.1 eV of its π energy upon vacancy formation, almost 0.80 eV are recovered by the bond shortening accompanying this relaxation.

We now turn to evaluate the role of the Q_θ and Q_ϵ Jahn-Teller distortion modes. These distortions will have a direct effect on the defect orbital through both linear and nonlinear Jahn-Teller coupling. Before giving the results of the calculation we briefly discuss the nature of the defect orbitals involved. The doubly degenerate e' defect orbital can be described using the defect molecule notation[21] by two orthogonal hybrid functions:

$$\Phi_\epsilon = (1/\sqrt{2})(\phi_a - \phi_b),$$
$$\Phi_\theta = (1/\sqrt{6})(2\phi_c - \phi_a - \phi_b), \tag{4}$$

where ϕ_a, ϕ_b, and ϕ_c denote sp^2 hybrids of the three dangling bonds associated with atoms a, b, and c, respectively (Fig. 8). It is immediately recognized that the asymmetric function Φ_ϵ is antibonding with respect to atoms a and b while the symmetric Φ_θ function is bonding between these atoms. Thus, an inward relaxation ($\gamma > 0$) along the Q_θ distortion mode would tend to stabilize Φ_θ and distabilize Φ_ϵ while an outward distortion would have the opposite effect. The energy gain associated with both distortions is equal in the linear approximation, however, nonlinear effects could favor one of them over the other.

Figures 11 (a) and (b) show the calculated properties related to Q_θ and Q_ϵ modes, respectively. It is seen that the Jahn-Teller binding energy gained by these distortions is very low ($E_B = -0.028$ eV for the θ mode and $E_B = -0.020$ eV for the ϵ mode), the Q_θ mode leading to a slightly lower energy for an outward distortion of -0.028 Å. Almost all the stabilization energy in the Jahn-Teller distortions is found to result from the σ levels, the defect level itself contributing most of it. Thus, owing to the relative rigidity of the σ skeleton, only a small amount of stabilization due to lattice relaxations results from the Jahn-Teller distortions while symmetric relaxations reveal a higher stabilization, mainly due to lowering of the π energy. Nonlinear coupling terms are found to contribute to the Q_θ Jahn-Teller energy, resulting in an asymmetric double well potential for this mode [Fig. 11(a)]. The way nonlinear terms enter the Jahn-Teller effect through the formalism of molecular orbital theory has been emphasized before.[68]

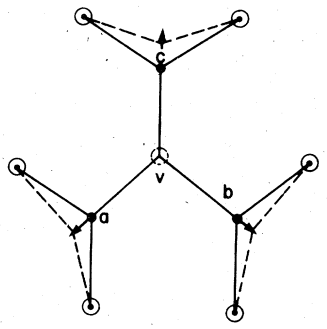

FIG. 10. Geometry of symmetric lattice relaxation. Full circles denote the nearest-neighbor atoms (labeled a, b, c) displaced in the direction of the arrows. Open circles—next-nearest-neighbor atoms. The broken lines denote schematically the shorter bonds formed after relaxation.

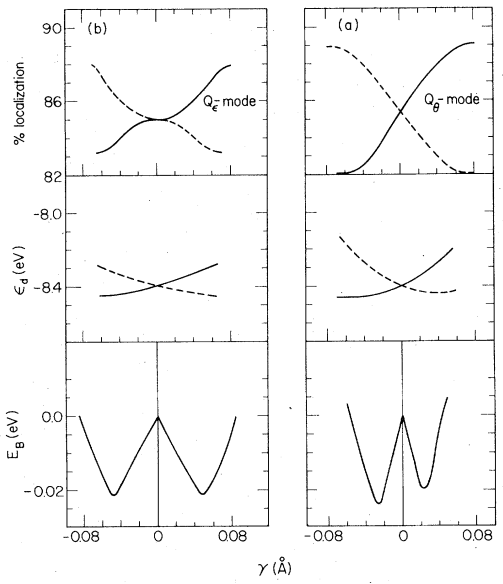

FIG. 11. Degree of localization of the defect wave function, energy (ϵ_d) of the vacancy level, and the vacancy binding energy (E_B) (relative to the unrelaxed vacancy). (a) Q_θ relaxation. (b) Q_ϵ relaxation.

Normalized amplitudes of distortion at equilibrium are:

$$Q_\theta^{\min} = \sqrt{6}\,\gamma_{\min}^{\theta} = 0.068 \text{ Å}$$

and

$$Q_\epsilon^{\min} = \sqrt{2}\,\gamma_{\min}^{\epsilon} = -0.068 \text{ Å}$$

compared with the value obtained for the a' distortion $Q_{a'}^{\min} = \sqrt{3}\,\gamma_{\min}^{a'} = -0.113$ Å. The degree of localization is shown to drop to about 83% due to the outward relaxation. The change in the localization due to lattice distortions [Figs. 11(a) and 11(b), top] follows different patterns in the Q_θ and Q_ϵ modes; while in the former case the take-off is characterized by a rather steep slope, in the latter case a vanishing initial slope is manifested.

The parameters characterizing the Q_θ-mode Jahn-Teller effect can be easily extracted from our numerical calculations (Fig. 11) using the standard form of the Jahn-Teller Hamiltonian.[69] From the mean depths of the wells in the bottom parts of Fig. 11(a) we obtain $E_{JT} \sim 0.023$ eV arising from the linear vibronic coupling, while the difference between the well depths or the comparison with the well depths in Fig. 11(b) yields the strength of the nonlinear coupling as $\beta \cong -0.04$ eV. The notation of Ref. 69 (see glossary there) is followed. The figures lead to a force constant of 1.2×10^5 dyn/cm compared to about 5.6×10^7 dyn/cm obtained (paper I) for the perfect lattice and to the value of $\approx 6.7\times10^5$ dyn/cm deduced from experiment for the regular lattice.[70] The vibrational motion in the well is characterized by $\omega = 410$ cm^{-1}. The rotational energy of the theory is $\alpha \cong 0.02$ eV so that the following ratios are derived:

$$E_{JT}/\hbar\omega = 0.45, \quad \beta/\alpha = -0.2,$$

indicating moderate linear and weak nonlinear coupling. Other vibronic parameters of the system (using the definitions of Ref. 69), are: $L \cong 0.082$ eV; $K \simeq 0.023$ eV, and $N \cong 0$, L, K, and N being the linear, quadratic, and cubic coupling coefficients, respectively. The numerical values given in this section involving as they do high-order energy derivatives, *must be accepted as merely approximative*. The following qualitative conclusions are, however, significant: the stable situation, corresponding to $\gamma < 0$ is one in which one carbon atom moves towards the vacancy and two move away from it, the stabilized ground state is the Φ_θ state rather than Φ_ϵ.

In the analogous system of a neutral vacancy in diamond, calculations within the rigid LCAO approximation using equilibrium spring constants deduced from the spectra of the regular solid[30] yielded $E_{JT} = 0.05$ eV. The substantial decrease in the force constant near the vacant site in graphite, as obtained here, implies that a force field transferred from the regular lattice data should furnish a rather poor approximation to the elastic response of the crystal near the perturbed site.

Since the $Q_{a'}$ and Q_θ modes are shown to be the most effective in lowering the energy of the system, we have minimized the energy with respect to a combined $Q_{a'}$ and Q_θ. This resulted in a slight improvement over the previous values, yielding a binding energy of -0.842 eV. At this final structure, atoms a and b are pulled by 0.10 Å away from the vacancy and atom c by 0.010 Å. This structure corresponds to a -3.5% shortening of each of the four bonds connecting atoms a and b with their carbon nearest neighbors, a shortening of -1.5% of the two bonds formed by atom c, an increase of $+6.9\%$ in the a-b bond and a 3.83% increase in the a-c and b-c bonds. The overall change in the bonds surrounding the vacancy is -1.6, or -0.18% per bond. The vacancy self-energy is reduced from the unrelaxed lattice value of 12.61 to 11.77 eV corresponding to an energy of vacancy formation of $E_{vf} = E_v - E_s = 11.77 - 7.40 = 4.37$ eV. The final structure obtained after minimizing the systems energy with respect to the $Q_{a'} + Q_\theta$ modes was subjected to a self-consistent treatment. This resulted in a decrease in the formation energy to 4.29 eV and a small increase in localization[63, 71] (86%). After consideration of

the uncertainties in the theoretical values of the promotion energies[63,71] and of the experimental error in determining the sublimation energy,[64,72] our calculated value for the vacancy formation in graphite is $E_{vf} = 4.0 \pm 0.5$ eV.

C. Comparison with experimental data and other calculations

In this section we compare our calculated results for the energy of vacancy formation, the basal plan contraction, and the position of defect level, with the available experimental evidence.

Several theoretical and experimental determinations of E_{vf} have been previously attempted. Annealing of vacancy loops has led Baker and Kelly[73] to deduce a value of $E_{vf} = 2.4-4.2$ eV while Henning[74] suggested a higher value of 6.6 eV using a vacancy decoration technique after quenching. Kanter[75] obtained a value of 7.1 eV for the activation energy of self-diffusion E_{sd}. Assuming that self-diffusion occurs via a vacancy mechanism and using the energy of vacancy migration E_{vm} of Diens[31] (3.1 eV) or the corrected value given by Kanter[75] (4.0 eV) the energy of vacancy formation was estimated as $E_{vf} = E_{sd} - E_{vm} = 4.0-3.1$ eV. More recent diffusion experiments of Thrower[76] have suggested $E_{vf} \approx 6.5$ eV. Our calculated value of $E_{vf} = 4.0 \pm 0.5$ eV lies between these values.

The vacancy-formation energy in graphite was previously calculated[21] in the defect molecule model. Neglecting small[77] interlayer binding effects, the unrelaxed vacancy formation energy was given by Coulson *et al.*[21] as:

$$E_{vf} = (3E_\sigma + \Delta E_\pi - E_{rel}) - E_{pro} - E_s , \tag{5}$$

where E_σ is the σ-overlap energy involved in breaking a σ bond in the valence sp^2 state, ΔE_π is the loss of π energy upon creation of a vacancy, E_{rel} is the electronic relaxation energy, (calculated for the three defect atoms using semiempirical configuration interaction), E_{pro} is the promotion energy from an atomic ^3P state to the sp^2 valence state, and E_s is the sublimation energy. Calculating the values of E_{rel} and ΔE_π in a defect molecule model, employing the value of E_{pro} given by Goldfarb and Jaffe[63] or Jordan and Longne-Higgins[71] and using the experimental values of E_s,[72] Coulson *et al.*[21] obtained $E_{vf} = 10.74-13.05$ eV. In this calculation the E_σ value was expressed by the quantities E_s, and E_{pro} and the calculated π energy per bond E_π.[21] Since we have employed the same E_{pro} and E_s values as Coulson *et al.* and obtained similar ΔE_π values (Coulson *et al.*, $\Delta E_\pi = 2.39$ eV; our value: $\Delta E_\pi = 2.1$ eV) one can compare the defect molecule (DM) and our (SPC) results writing $(3E_\sigma - E_{rel})_{DM} = 25.1-27.4$ eV and $(3E_\sigma - E_{rel})_{SPC} = 18.7$ eV. The discrepancy between the defect molecule result and ours can only be partially attributed to an increase in E_{rel} in the present study (self-consistency and lattice relaxation, not introduced in the defect molecule calculation are shown here to reduce the energy by 1.8 and 0.86 eV, respectively). The main source of discrepancy lies in the high value of E_σ implied by the defect molecule calculation [8.66 eV obtained from Eq. (5)]. In a later study, Coulson and Poole[22] used a much lower value for E_σ (6.81 eV) which is very close to the value suggested by Walsh.[78] Using this value one obtains $(3E_\sigma - E_{rel})_{DM} = 17.2-19.5$ eV and $E_{vf} = 7.5-5.2$ eV. Self-consistency and relaxation corrections would, if anything tend to bring this value closer to our estimate.

Recently, Phillips and Van Vechten[79] have suggested a macroscopic model for calculating E_{vf} in diamond-type semiconductors. In his model the energy of vacancy formation is given by

$$E_{vf} \cong \Delta F_v^m + \Delta E^{ms} . \tag{6}$$

ΔF_v^m is the energy required to remove an atom from a linearly screened medium characterized by spherically symmetric metallic bonds with no directed bonding charge. This term is approximated by the surface energy involved in the formation of a vacancy bubble of radius r_w in the liquid state and is calculated from the measured surface energy per area σ according to[79]:

$$\Delta F_v^m = 4\pi r_w^2 \sigma , \tag{7}$$

where r_w is the atomic Wigner-Seitz radius. ΔE^{ms} is the anisotropic formation energy denoting the energy required to form the directional dangling bonds from the tails of the spherical metallic charge distribution through nonlinear screening effects. For the diamond structure this bond formation energy is approximated by the energy of white-tin to diamond transition and was phenomenologically calculated by Van Vechten.[80] This model can be extended to the graphite structure to obtain estimates of E_{vf}. Using the average of the basal plane and c-plane surface energies of graphite given by Abrahamson[81] to approximate the isotropic bubble energy ($\sigma_{av} \cong 2480$ erg/cm^2) one obtains $\Delta F_v^m = 1.98$ eV. The correction term ΔE^{ms} (calculated by Van Vechten to be 2.36 eV for four covalent bonds in diamond or ≈ 1.77 eV for $Z = 3$) has no direct phenomenological analog in the graphite structure, however, owing to the higher nonlinear screening effects in graphite (as manifested by larger dispersion theory[82] bond charges in the latter, i.e., $Z_{b\sigma} = -0.21e$ in graphite compared with $Z_b = -0.17e$ in diamond[82] and higher average band gaps in the Penn model,[60] i.e., $E_g^\sigma = 15$ eV compared with[82] $E_g = 13.6$ eV in diamond) one

would expect a slightly larger ΔE^{ms} value in graphite. These arguments would suggest roughly $E_{vf} \approx 4$ eV in graphite.

Both the macroscopic model and the corrected defect molecule model lead to values of E_{vf} that are in substantial agreement with that of the present study. Phenomenological models using various forms of atom-atom potentials seem rather crude for systems containing both a relatively rigid σ skeleton and a polarizable π system. It has been realized some time ago[83,84] that simple atom-atom potentials that neglect the many-body coupling of the atoms surrounding the given atomic pair, fail to predict the stable conformation and the correct lattice dynamics of aromatic and ionic crystals and one has to introduce a quantum-mechanical description of the role of the delocalized π system on the potential surface.

The average theoretical contraction $\Delta a/a$ of the basal plane of graphite due to relaxation of the atoms around a single vacancy, was calculated in the present work to be -0.18% per bond. The observed[3] value $(\Delta a/a)_{obs}$ obtained by irradiating at -196 °C (where defect aggregation is assumed to be very small) can be partitioned into a contribution originating from a Poisson-ratio effect[85,86] denoted $(\Delta a/a)_{Poisson}$ and to the vacancy-induced relaxation part $(\Delta a/a)_{vac}$. The former contribution arises from the increase in the c spacing $\Delta c/c$ due to interstitial formation and is proportional to the compliance ratio S_{13}/S_{33}, i.e., $(\Delta a/a)_{Poisson} = (\Delta c/c)(S_{13}/S_{33})$. Using the observed Poisson ratio[86] and the $\Delta c/c$ and $\Delta a/a$ values measured by Pluchery[3] and by Henson and Reynolds,[2] one obtains $(\Delta a/a)_{vac} \sim -(0.13-0.05)\%$. Only rough agreement is obtained with the present extended-Hückel SPC calculation. Using an average bond-order bond-length correlations[87] in a simple π-electron model, Kelly[85] obtained a theoretical estimate of $C_v^{-1}(\Delta a/a)_{vac} = -0.14$ where C_v^{-1} is the number of atoms associated with each vacancy. Since in our model only the bonds involving the three nearest and six next-nearest neighbors are affected by the presence of the vacancy (i.e., $C_v^{-1} = 9$), our results can be written approximately as $C_v^{-1}(\Delta a/a)_{vac} \sim -0.144$ in good agreement with Kelly's suggestion. It thus seems that although the simple semiempirical LCAO technique employed here is too crude for obtaining realistic atomic conformations at equilibrium, the overall expected trends are correctly reproduced.

The energetic position of the vacancy level with respect to the valence crystal bands can not at present be conclusively compared with experiment, owing to the lack of detailed optical spectra of irradiated graphite. A preliminary study of the optical spectra of neutron irradiated graphite[88] at 80 °C revealed an absorption at 2.6 eV that disappears completely upon annealing and is not present in the unirradiated samples. Since only neutral vacancies are expected to be stable at normal conditions,[21] the assignment of the observed transition to a negative vacancy[88] seems doubtful. The transition between the ground state of the neutral vacancy to the lower excited state $({}^2E \rightarrow {}^2A_1')$ was calculated by Coulson *et al.*[21] to occur at 7.7–5.0 eV while the analogous transition in our model (between the point of the highest density of states in the a' system to the e' defect level) is 5 eV. The transition between the edge of the σ bands to the defect level is calculated in our model to occur at slightly lower energy (4.0 eV in the unrelaxed lattice and 3.55 eV in the minimum conformation) and can be tentatively assigned to the observed transition. More experimental studies on the optical spectra of vacancy-containing graphite are doubtless necessary before definite assignment can be made.

D. Vacancy migration energy and displacement threshold

To complement the study of a removal of an atom from its crystalline site to the surface (vacancy formation), we study the effects associated with placing the removed atom inside the layer plan (atomic displacement) and moving the vacancy itself (vacancy migration).

The model adopted for studying the vacancy migration energy E_{vm} is schematically revealed in Fig. 12. After the removal of the central atom from position B the system has the total energy denoted E_{vac}. The atom initially located at site A is then allowed to move toward the vacant site. The excess energy involved in this process over the

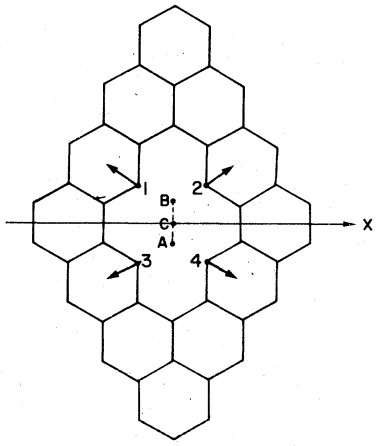

FIG. 12. Geometry of the model used to calculate the activation energy for vacancy migration in the $C_{49}V$ periodic cluster.

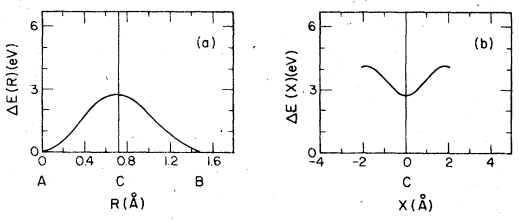

FIG. 13. (a) Activation energy for vacancy migration in the unrelaxed lattice. The displaced atom moves along the A-C-B axis (Fig. 12). (b) Activation energy for vacancy migration in the unrelaxed lattice. The displaced atom moves along the X axis (Fig. 12).

energy E_{vac} is denoted $\Delta E(R)$ where R denotes the position of the displaced atom along the line A-C-B. The calculated function $\Delta E(R)$ is shown in Fig. 13(a). Positions A and B are equivalent and are characterized by $\Delta E(R_A) = \Delta E(R_B) = 0$ while the maximum ΔE value is maintained at site C lying midway between points A and B. The activation energy of vacancy migration in this unrelaxed configuration is calculated to be 2.79 eV. Displacement of the atom at site C, along the X direction, perpendicular to the A-C-B direction (Fig. 12) reveals an increase in the energy ΔE, showing that C is a saddle point [Fig. 13(b)]. We now allow for relaxation effects on both the initial configuration ($E_{in} = E_{vac}$) and the saddle-point configuration ($E_{fi} = E_{vac} + \Delta E$). Symmetric a' relaxation coupled with θ-mode Jahn-Teller distortions were shown (Sec. IV B) to stabilize the initial configuration by 0.842 eV. To allow for relaxations in the saddle-point configuration, the atoms labeled 1, 2, 3, 4 in Fig. 12 are allowed to relax when the displaced atom is at C. The energy E_{fi} is minimized as a function of the relaxation amplitude. This results in a lowering of 0.387 eV for an outward relaxation of 0.08 Å. Relaxations in the initial vacancy configuration are thus more effective in lowering the energy than relaxations in the saddle-point configuration, resulting in a final activation energy of vacancy migration of 3.25 eV. This agrees favorably with the experimental value $E_{vm} = 3.15 \pm 0.55$ eV given by Baker and Kelly,[73] with the estimate $E_{vm} > 2.5$ eV given by Henson and Reynolds[2] and with $E_{vm} \cong 3$ eV given by several authors.[76, 89] Assuming that self-diffusion in graphite occurs via a vacancy mechanism, one would obtain an activation energy to self-diffusion of $E_{vf} + E_{vm} = 7.3 \pm 0.5$ eV which is in reasonable agreement with the measured values of 7.1 ± 0.5 eV,[75] and 8.3 ± 0.3 eV.[76]

We next turn to evaluate the threshold energy of atom displacement in graphite. This is done by calculating the change in the total lattice energy upon removing a carbon atom from a substitutional site and placing it at some distant site. Displacement along the open direction (X-direction in Fig. 12) would not involve high barriers and is thus favored. Figure 14 depicts the amount of energy necessary to move an atom that was initially at site A, to various sites along the open direction. From this, a displacement threshold of about $E_d^{\perp} = 21.4$ eV for the C_{32} cluster and $E_d^{\perp} = 21.8$ eV for the C_{50} cluster could be deduced. Similarly, the displacement threshold perpendicular to the basal plane is calculated to be $E_d^{\parallel} = 19.6$ eV in the two-dimensional lattice. This value would probably increase substantially in the three-dimensional lattice due to interaction with atoms from other layers. The evaluation of E_d by the periodic cluster method is limited by the need to consider only small separations between the constituents of the Frenkel pair due to the superlattice representation involved. A similar calculation with a truncated cluster of 50 atoms having the same geometry as our C_{50} basic cell and no periodic boundary conditions, yields $E_d^{\perp} = 22.3$ eV (a value of 25.3 eV has been previously obtained by Moore and Carlson[90] using a 36-atom truncated cluster and an unmodified extended-Hückel scheme[91]). These calculated values correspond to the unrelaxed lattice and assume that the displaced atom does not undergo the sp^2 transition during displacement. Introduction of dynamical relaxation effect would probably lower these calculated values.

Early experimental determinations of the displacement threshold in graphite, yielded values around 25–33 eV,[92, 93] while Lucas and Mitchell ob-

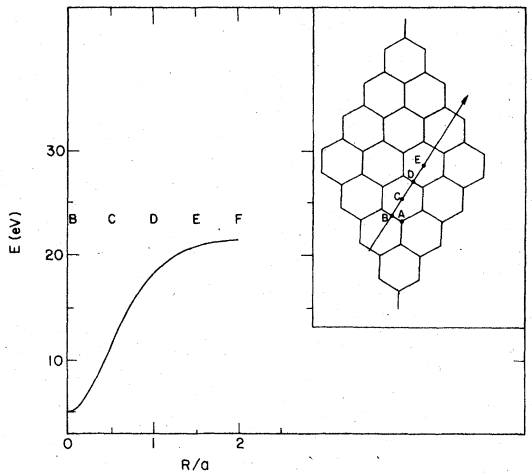

FIG. 14. Plot of the energy required to move the atom that was initially at the substitutional site A (Fig. 12) to various points in the layer plane. R measured in units of the lattice constant $a = 2.46$ Å.

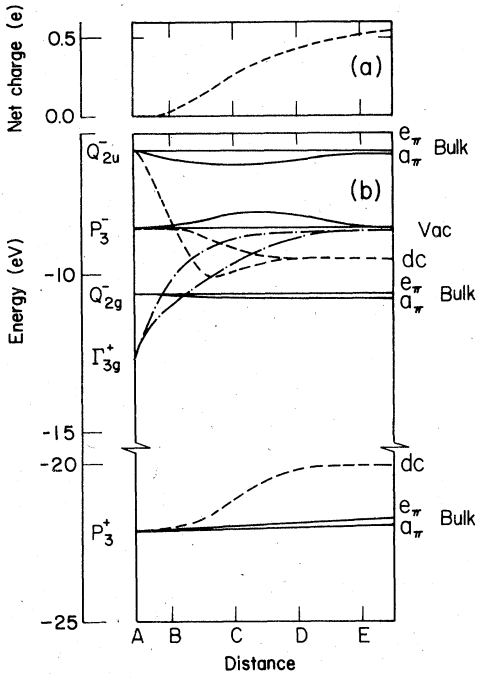

FIG. 15. (a) Net charge on displaced atom. (b) Dependence of some one-electron energy levels on the separation between the constituents of the Frenkel pair. See text for notation. The letters on the X axis denote positions of the displaced carbon as labeled in the insert to Fig. 14. Solid line—bulk levels; dashed line—displaced site levels; dashed-dot—vacancy levels.

tained a much higher value of 60 ± 10 eV.[6] A recent reexamination by Montet indicated a value as low as 27.9 eV.[94] The latter author indicates[95] that much higher values are associated with displacement by electron beams that form aligned 60°–90° with respect to the C axis[96] while normal incidence reveals displacement thresholds that are consistent with previous determinations other than that of Lucas and Mitchell.[6] Our calculated result agrees favorably with this determination.

The variation of some of the high-symmetry one-electron levels in the crystal upon displacement of the carbon atom in the basal plane, is revealed in Fig. 15. The direction of displacement is denoted in the insert to Fig. 14. The atom at the origin (site A) is displaced to the positions labeled B-E thus increasing the separation of the Frenkel pair from 0.71 Å (position B) to 1.42, 2.56, and 3.76 Å (positions C, D, and E, respectively). The one-electron energy levels can be classified into three groups: the levels denoted dc whose wave function resides mainly on the displaced carbon atom, the levels denoted Vac that represent at the limit of large separation the doubly degenerate e' vacancy level, and the levels labeled Bulk representing delocalized crystal levels.

The displaced carbon levels are associated with wave functions that are highly localized on the displaced site and are thus constructed from many states in the BZ; however, their *parentage* in terms of single isolated states in the BZ of the perfect lattice, can be identified by following the variation in the energy and wave functions of perfect lattice states as a function of the displacement. It is thus seen that a displaced carbon level having mainly $2s$ character evolves from the low σ bands of the regular lattice at the point P_3^+ while $2p$-type levels associated with the displaced atom originate from the Q_{2u}^- and P_3^- states. Similarly, the vacancy e' level appearing at high separation between the hole and the displaced atom is highly localized on the three nearest-neighbors to the vacant site and originates from the doubly degenerate Γ_{3g}^+ state in the valence band of the perfect lattice. Other levels of the perfect lattice may split or shift due to the Frenkel-pair formation; however, these changes in energy and the accompanying changes in the wave functions, are very small (of the order of N^{-1} where N is the cluster size). It is perhaps worth mentioning that as the carbon atom is displaced from its substitutional site, it loses some electronic charge and maintains a positive net charge [Fig. 15(a)]. Large charge redistribution effects are manifested by carbon displacements and many self-consistent iteration cycles (10–15) are needed to obtain convergence in the charges. The self-consistent results exhibit a net charge of the order of $+0.5e$ on the displaced carbon indicating that the Frenkel pair really corresponds to a vacancy-charged atom pair. The charge redistribution effects around the displaced atom reduces the calculated displacement threshold energy by 2.8 eV relative to the uniterated results, and the net atomic charge on the displaced atom by a factor of 2–2.5. Coulomb attraction forces and polarization effects[97] have thus to be introduced in non-self-consistent calculations[90, 98, 99] of such effects.

V. SUMMARY AND CONCLUSION

In the present work we have employed a small periodic cluster superlattice representation to the point-defect problem in graphite using an all-valence electron self-consistent LCAO scheme that has been previously shown to yield a good representation of the electronic properties of the regular solid. Eight crystal bands, 54–96 $\vec{k}$ points in the Brillouin zone and 2^2–5^2 primitive unit cells are allowed to interact in a nonperturbative calculation. The undesired defect–defect interaction

present in the superlattice model is shown to be effectively suppressed when the defect–defect separation reaches about three lattice constants. At this limit we calculate the electronic density of states, the charge distribution, the electrostatic vacancy potential, and the effect of both symmetric and Jahn-Teller lattice distortions.

The defect level is shown to be located some 3.5 eV above the top of the σ valence band and its wave function reveals some 80% localization on the three nearest neighbors. The wave function is mostly $2p_\sigma$ like but contains also some admixture of $2s$ character arising from the lower valence bands. The vacancy formation energy E_{vf} is calculated to be 4.9 ± 0.5 in the unrelaxed lattice and 4.0 ± 0.5 eV in the relaxed lattice.

Jahn-Teller Q_θ mode relaxation seems to be the dominant nonsymmetric stabilizing distortion revealing $E_{JT} = -0.023$ eV and a relaxation amplitude of -0.068 Å. Combined Jahn-Teller Q_θ and symmetric $Q_{a'}$ relaxation lower the total energy by -0.84 eV and induce an average bond shortening of -1.6%. The energy of vacancy migration is calculated to be $E_{vm} = 3.25$ eV and the Frenkel-pair formation energy is 22 eV. Owing to the approximate character of the semiempirical LCAO method used here, these estimates are not to be considered as definitive.

Some of the more general results are:

(a) Although graphite is a semimetal due to the degeneracy of its π valence and conduction bands at the BZ corner, it could be viewed as a high-gap insulator in its σ subsystem and hence can reveal true localized gap states upon defect formation.

Defect molecule models that treat only a small number of dangling bonds around the vacant site are bound to distort the vacancy wave function due to its relatively long tails. Coupling with the Bloch states of the crystal, not included in the defect molecule treatment, are shown to be important in such wide-band materials and play an important role in determining the redistribution of the vacancy levels among the crystal band states. Deep defect levels such as that treated here are in general not amenable to effective-mass theories due to the importance of the deep short part of the potential.

(b) Introduction of charge self-consistency is shown to stabilize the energy of the nonlocalized band states, to shift the defect level to the region of low density of states at the Fermi level and to increase its localization. The substantial charge redistribution effects manifested by the iterative calculation, suggest that self-consistency is essential even for homonuclear systems such as graphite. Average dielectric screening neglecting local-field corrections would probably be poor approximations in view of the strong charge perturbations observed here.

(c) The eigenvalue spectrum of the defect containing crystal is stabilized after introducing some 50 $\vec{K}$ points and 3–5 shells of atoms around the defect site. The localized defect wave function assuming contributions from several Bloch states is thus not amenable to calculation by methods restricting the number of translational irreducible representations and interacting cells to small numbers.

(d) Many-electron effects are probably very small for the vacancy ground state due to the single occupancy of the defect level and the substantial delocalization of the a' defect modes. Mixing with higher-energy many-electron configurations would similarly be small owing to the relatively large separation between the zero-order states. Correlation effects are, however, important in the excited states of the vacancy when two electrons populate the defect orbitals.

(e) Owing to accumulation of excess π charge on the atoms surrounding the vacancy these bonds relax to a shorter bond configuration in a $Q_{a'}$ deformation mode. Jahn-Teller deformation, on the other hand, affects mainly the degenerate modes that belong to the σ system. Owing to the relative rigidity of the σ skeleton such relaxations are small being characterized by low Jahn-Teller energies and medium to low linear and nonlinear coupling coefficients.

(f) Owing to an incorporation of both the nonlocalized band states and the defect states in a self-consistent treatment, the SPC method is capable of revealing various defect formation energies as well as correlating the level position of the defect states with the perfect lattice band structure. The use of more rigorous one-electron methods to replace the simple LCAO scheme used here would no doubt help to assess the validity of our results.

---

*Present address: Department of Physics, Northwestern University, Evanston, Illinois 60201.

[1]R. J. Price and J. C. Bokros, Carbon 5, 73 (1967).

[2]R. W. Henson and W. N. Reynolds, Carbon 3, 277 (1965).

[3]M. Pluchery, in *Radiation Damage in Reactor Materials* (IAEA, Vienna, 1963), p. 523.

[4]E. W. J. Mitchell and M. R. Taylor, Nature 208, 638 (1965).

[5]P. R. Goggin and W. N. Reynolds, Philos. Mag. 8, 265 (1963).

[6]M. W. Lucas and E. W. J. Mitchell, Carbon 1, 345

(1963).
[7]J. H. Crawford and L. M. Slifkin, *Point Defects in Solids* (Plenum, New York, 1972).
[8]W. Kohn and J. M. Luttinger, Phys. Rev. 97, 1721 (1955).
[9]G. D. Watkins, in *Radiation Damage and Defects in Semiconductors* (The Institute of Physics, London, 1973), p. 228.
[10]R. J.Cook and D. H. Whiffen, Proc. R. Soc. A 295, 99 (1966).
[11]G. D. Watkins, J. Phys. Soc. Jpn. Suppl. 18, 22 (1963).
[12]G. F. Koster and J. C. Slater, Phys. Rev. 95, 1167 (1954); 96, 1208 (1954).
[13]J. Callaway and A. J. Hughes, Phys. Rev. 156, 860 (1967); 164, 1043 (1967).
[14]M. Jaros and S. F. Ross, J. Phys. C 6, 1753 (1973); 6, 3451 (1973).
[15]C. A. Coulson and M. J. Kearsley, Proc. R. Soc. A 241, 433 (1957).
[16]T. Yamaguchi, J. Phys. Soc. Jpn. 17, 1359 (1962); 18, 368 (1963).
[17]J. Callaway and A. J. Hughes, *Radiation Effects in Semiconductors*, edited by F. Vook (Plenum, New York, 1968), p. 27.
[18](a) R. P. Messmer and G. D. Watkins, Phys. Rev. B 7, 2568 (1973). (b) R. P. Messmer and G. D. Watkins, in *Radiation Damage and Defects in Semiconductors* (The Institute of Physics, London, 1973), p. 255. (c) G. D. Watkins and R. P. Messmer, Phys. Rev. Lett. 32, 1244 (1974).
[19]F. P. Larkins, J. Phys. C 4, 3065 (1971); 4, 3077 (1971).
[20]A. Baldereschi and J. J. Hopfield, Phys. Rev. Lett. 28, 171 (1972).
[21]C. A. Coulson, M. A. Herraez, M. Leal, E. Santos, and S. Senent, Proc. R. Soc. A 274, 461 (1963).
[22]C. A. Coulson and M. D. Poole, Carbon 2, 275 (1964).
[23]K. Weiser, Phys. Rev. 126, 1427 (1962).
[24]A. B. Lidiard, *Radiation Damage and Defects in Semiconductors* (The Institute of Physics, London, 1973), p. 238.
[25]M. Lannoo, Phys. Rev. B 10, 2544 (1974).
[26]E. L. Elkin and G. D. Watkins, Phys. Rev. 174, 881 (1968).
[27]G. D Watkins, in *Radiation Effects in Semiconductors*, edited by F. L. Vook (Plenum, New York, 1968), p. 67.
[28]C. A. Coulson, *Radiation Damage and Defects in Semiconductors* (The Institute of Physics, London, 1973), p. 249.
[29]F. P. Larkins, J. Phys. Chem. Solids 32, 965 (1971); 32, 2123 (1971).
[30]J. Friedel, M. Lannoo, and G. Leman, Phys. Rev. 164, 1056 (1967).
[31]G. J. Dienes, J. Appl. Phys. 23, 1194 (1952).
[32]P. A. Swalin, J. Phys.Chem. Solids 18, 290 (1961).
[33]C. A. Coulson, S. Senent, M. A. Herraez, M. Leal, and E. Santos, Carbon 3, 445 (1966).
[34]A. Zunger, J. Phys. C 6, 96 (1974).
[35]A. Zunger, J. Chem. Phys. 62, 1861 (1975).
[36]A. Zunger and A. Katzir, Phys. Rev. B 11, 2378 (1975).
[37]A. Zunger, J. Chem. Phys. 63, 1713 (1975); R. Englman and A. Zunger Bull. Am. Phys. Soc. (to be published March 1976).
[38]S. L. Cunningham, Phys. Rev. B 10, 4988 (1974).
[40]The calculation of the Peierls instability in the one-dimensional $(SN)_x$ crystal (Ref. 4) and the calculation of the collective-motion force constants in solid hydrogen flouride (Ref. 37) are performed by calculating the total crystal energy where a superlattice of conformational changes is introduced in an enlarged unit cell.
[41]A. Zunger, J. Chem. Phys. 63, 4854 (1975).
[42]R. Siems, Phys. Status Solidi 30, 645 (1968).
[43]M. H. Yoo, Phys. Status Solidi 61, 411 (1974).
[44]J. C. Stoddart, N. H. March, and J. M. Stott, Phys. Rev. 186, 683 (1969).
[45]A. D Boardman, M. I. Darby, and E. T. Micah, Carbon 11, 207 (1973).
[46]In the course of the computational work, it was found that considerable computing time could be saved if an initial small cluster (C_7V-6$\vec{k}$) is first treated (using proper damping of the iteration cycle) and the charge distribution over the various sites obtained at the final iteration, is subsequently transferred to a larger cluster as an initial guess. The atoms in the larger cluster, not appearing in the smaller one are assumed to be neutral in the first iteration. In this manner, 5-6 iterations for the smaller clusters and 2-4 iterations in the larger cluster were sufficient to obtain convergence.
[47]T. Shimizu and K. Minami, Phys. Status Solidi B 62, 585 (1974).
[48]In the present study, the Löwdin charge definition was used. This was preferred over the Mulliken definition (Ref. 49) that apportions the bond charge equally between the atoms. Previous studies on molecules (Ref. 50–52) have been indicated that self-consistent treatment based on the Löwdin charges, yields better results for the dipole moments and one-electron energies. Owing to the orthogonality of the basis in the Löwdin representation, the resulting wave functions are less localized than the corresponding nonorthogonal functions used in the Mulliken charge definition and hence the Löwdin charges are usually smaller than the Mulliken charges. The converged Mulliken net atomic charge on a carbon nearest to the vacancy was 0.21e compared with the Löwdin charge of 0.16e.
[49]R. S. Mulliken, J. Chem. Phys. 23, 1833 (1955).
[50]E. W Stout and P. Politzer, Theor. Chim. Acta 12, 379 (1968).
[51]M. Miznno and S. Saeki, Mol. Phys. 24, 219 (1972).
[52]A. H. Harker, J. Phys. C 7, 3224 (1974).
[53]D. S. Billington and J. H. Crawford, *Radiation Damage in Solids* (Princeton U.P., New York, 1961), p. 394.
[54]G. H. Kinchin, J. Nucl. Energy 1, 124 (1954).
[55]L. C. Blackman, G. Saunders, and A. P. Ubbelhode, Proc. Phys. Soc. Lond. 78, 1048 (1961).
[56]G. Wagoner, Bull. Am.Phys. Soc. 6, 129 (1961); *Proceedings of the Fourth Conference on Carbon* (Pergamon, New York, 1960), p. 197.
[57]K. A. Müller, Phys. Rev. 123, 1550 (1961).
[58]J. E. Hove, Phys. Rev. 100, 1806 (1955).
[59]J. E. Hove and J. D. McClelland, J. Chem. Phys. 26, 1028 (1957).
[60]It is interesting to observe that due to the accumula-

tion of charges of opposite signs on the three nearest-neighbor and on the six next-nearest-neighbor atoms, the Madelung-type terms appearing in the diagonal matrix elements [third term in Eq. (6) paper I)] cancel approximately and one is left with the situation where the diagonal element is approximately given by $F^{\alpha\alpha}_{\mu\mu}(q_\alpha) \cong F^{\alpha}_{\mu}(0) - q_\alpha \Delta^{\mu}_{n\alpha,n\alpha}$. Thus, due to the special nodal character of the wave function involved, the simple iterative-extended-Hückel scheme furnishes a reasonable first approximation to the full Hamiltonian [Eq. (6) paper I)]. This should partially explain the success of the iterative-extended Hückel calculations on point defect in graphite (Ref. 35). In calculations on the optical properties of *binary* hexagonal boron nitride, it was found (Ref. 62) that cancellation occurs in the sum of the linear $q\Delta$ term and the Madelung-type terms due to the alternating signs of the charge on the two chemically different sublattices. In this case the diagonal element $F^{\alpha\alpha}_{\mu\mu}(q_\alpha)$ is approximately given by $F^{\alpha}_{\mu}(0)$ and hence the simple Hückel becomes a good approximation.

[61]K. H. Bennemann, in *Lattice Defects in Semiconductors*, edited by R. H. Hasiguti (University of Tokyo Press, Tokyo, 1968), p. 30; Phys. Rev. 137, A1497 (1965).

[62]A. Zunger, A. Katzir, and A. Halperin, Phys. Rev. B 13, 5560 (1975).

[63]I. J. Goldfarb and H. H. Jaffe, J. Chem. Phys. 30, 1912 (1959).

[64]P. D. Zavitsanos and G. A. Carlson, J. Chem. Phys. 59, 2966 (1973).

[65]W. Jones and N. H. March, *Theoretical Solid State Physics* (Wiley, New York, 1973), p. 985–988.

[66]F. P. Boer, M. D. Newton, and W. N. Lipscomb, Proc. Natl. Acad. Sci. U. S. 52, 890 (1964).

[67](a) A. Seeger and M. L. Swanson, in *Lattice Defects in Semiconductors*, edited by R. R. Hasiguti (University of Tokyo Press, Tokyo, 1968), p. 93. (b) R. R. Hasiguti, *ibid.*, p. 131.

[68]M. D. Sturge, *Solid State Physics*, edited by F. Seitz, D. Turnbull, and H. Ehrenreich (Academic, New York, 1967), Vol. 20, p. 90.

[69]R. Englman, *The Jahn Teller Effect in Molecules and Crystals* (Wiley, London, 1972).

[70]K. K. Mani and R. Ramani, Phys. Status Solidi B 61, 659 (1974).

[71]P. C. H. Jordan and H. C. Longnet-Higgins, Mol. Phys. 5, 121 (1962).

[72]H. T. Knight and J. P. Rink, J. Chem. Phys. 29, 449 (1958).

[73]C. Baker and A. Kelly, Nature 193, 235 (1962).

[74]C. Hennig, J. Appl. Phys. 36, 1482 (1965).

[75]M. A. Kanter, Phys. Rev. 107, 655 (1957).

[76]P. A. Thrower, Philos. Mag. 18, 697 (1968).

[77](a) R. O. Brennan, J. Chem. Phys. 20, 40 (1952). (b) E. Santos and A. Villagra, Phys. Rev. B 6, 3134 (1972).

[78]A. D. Walsh, Trans. Faraday Soc. 43, 60 (1947).

[79]J. C. Phillips and J. A. Van Vechten, Phys. Rev. Lett. 30, 220 (1973).

[80]A. Van Vechten, Phys. Status Solidi B 42, 761 (1971).

[81]J. Abrahamson, Carbon 11, 337 (1973).

[82](a) J. C. Phillips, Rev. Mod. Phys. 42, 317 (1970); (b) Phys. Rev. 168, 912 (1968).

[83]A. Warshel and M. Karplus, J. Am. Chem. Soc. 94, 5612 (1972).

[84]M. Wagner and D. Kuhner, Z. Phys. 251, 300 (1972).

[85]B. T. Kelly, Nature 207, 257 (1965).

[86]H. W. Davidson and H. Losty, *Mechanical Properties, of Nonmetallic Brittle Materials* (Butterworths, London, 1958).

[87]M. Bradburn, C. A. Coulson, and G. S. Rushbrooke, Proc. R. Soc. Edinburgh A 62, 336 (1948).

[88]T. Iwata and Y. Sato, J. Phys. Soc. Jpn. 23, 1425 (1967).

[89]G. R. Hennig, in *Proceedings of the Second Conference on Industrial Carbon and Graphite* (Society of Chemical Industry, London 1965), p. 109.

[90]E. B. Moore and C. M. Carlson, Solid State Commun. 4, 47 (1965).

[91]R. Hoffman, J. Chem. Phys. 39, 1397 (1963).

[92]G. R. Hennig and J. E. Hove, in *Proceedings of the First Conference on the Peaceful Uses of Atomic Energy*, Geneva (United Nations, New York, 1955), Vol. 7, p. 751.

[93]D. T. Eggen, North Amer. Aviation Report NAA-SR-69, 1955 (unpublished).

[94]G. L. Montet, Carbon 11, 89 (1973).

[95]G. L. Montet, Carbon 5, 19 (1967).

[96]T. Ewata and T. Nihira, Phys. Lett. 23, 631 (1966).

[97]J. K. Weiser, Phys. Rev. 126, 1427 (1962).

[98]J. W. Corbett, J. C. Bourgoin, and C. Weigel, *Radiation Damage and Defects in Semiconductors* (The Institute of Physics, London, 1973), p. 1.

[99]C. Weigel, D. Peak, J. W. Corbett, G. D. Watkins, and R. P. Messmer, Phys. Rev. B 8, 2906 (1973).